Nanometer space resolved photochemistry

Steven De Feyter,[a] Johan Hofkens,[a] Mark Van der Auweraer,[a] Roeland J. M. Nolte,[b] Klaus Müllen[c] and F. C. De Schryver*[a]

[a] *Katholieke Universiteit Leuven (K.U.Leuven), Department of Chemistry, Celestijnenlaan 200 F, B-3001 Heverlee, Belgium. E-mail: frans.deschryver@chem.kuleuven.ac.be*
[b] *University of Nijmegen, Department of Organic Chemistry, NSR Center, Toernooiveld, 6525 ED Nijmegen, The Netherlands*
[c] *Max-Planck-Institut für Polymerforschung, Ackermannweg 10, D-55021, Mainz, Germany*

Received (in Cambridge, UK) 23rd November 2000, Accepted 31st January 2001
First published as an Advance Article on the web 23rd February 2001

The development of scanning probe techniques has opened new ways to visualize and gain insight in chemical and physical processes with unprecedented spatial resolution. Scanning near-field optical microscopy combining high spatial topographic resolution and optical resolution surpassing the diffraction limit, has been applied for structure determination and manipulation studies of organic materials. With scanning tunnelling microscopy, photo-induced chemical reactions have been studied at the liquid/solid interface with subnanometer resolution.

Introduction

The birth of scanning probe techniques revolutionized the way small objects or domains can be visualized. Common to all scanning probe techniques is a tiny probe, which scans a surface at a very small distance from it and the interaction between probe and object is translated into a signal. The ultimate control in positioning has been achieved by using piezoelectric elements. Since the invention of the scanning tunnelling microscope (STM),[1] several experimental schemes have been developed which allow detection of a great variety of interactions between probe and surface. Among those techniques, scanning near-field optical microscopy (SNOM)[2,3] takes a special place due to its optical resolution below the diffraction limit.

In STM, a metallic tip is brought very close to a conductive substrate and by applying a voltage between both conductive media, a tunnelling current may result (Fig. 1A). The exponential distance dependence of the tunnelling current provides excellent means to control the distance between the probe and the surface. Very high resolution (atomic) can be achieved but in general, the use of this probe technique is limited to conductive substrates. In contrast, in atomic force microscopy (AFM) forces exerted by the sample on the tip are recorded and several detection schemes are possible. In addition, modification of tips with carbon nanotubes leads to supertips with enhanced spatial and mechanical properties[4] and chemically modified AFM tips provide chemical contrast and can allow the measurement of binding forces.[5]

SNOM combines both the possibilities of AFM and optical microscopy. On the one hand, it allows for probing the surface and obtaining information on the topography. On the other hand, in aperture SNOM, the probe contains an aperture and the sample can be illuminated very locally (Fig. 1B). The diameter of the aperture at the end of the probe is typically of the order of 50–100 nm and therefore the illuminating spot is not diffraction limited. Both transmission and fluorescence in combination with polarization provide appropriate contrast mechanisms. The high sensitivity of this technique has been demonstrated by its ability to detect even single molecules.[6,7]

Frans De Schryver obtained his doctoral degree at K.U.Leuven in 1964 and returned as staff member to his Alma Mater after a two-year postdoctoral stay as a Fulbright fellow at the University of Arizona with Speed Marvel. He became a Full Professor in 1975 working in the field of photochemistry and photophysics. He received a Humboldt research award in 1993 and stayed with G. Wegner and J. P. Rabe at the Max-Planck-Institute for Polymer Research in Mainz. As a result of this stay he combined space and time resolution in the study of organic molecules. He received the Porter medal in 1998 and the Havinga medal and Forster memorial lecture award in 1999.

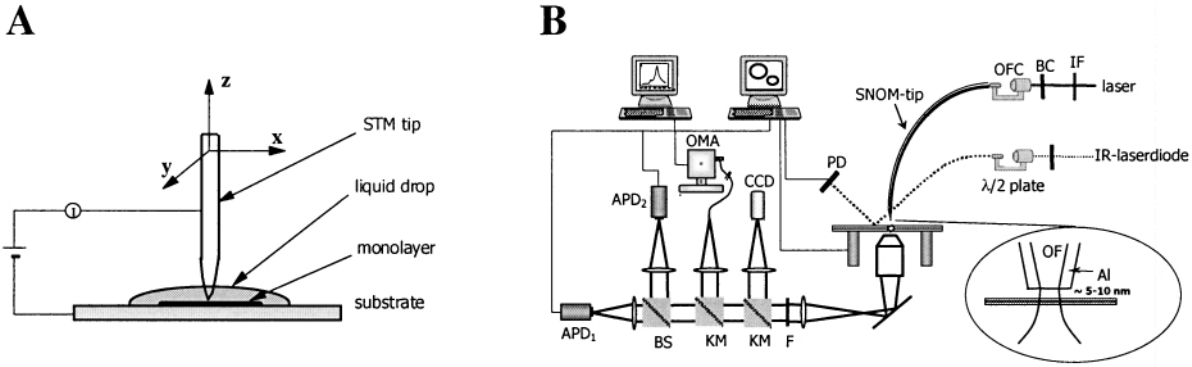

Fig. 1 (A) Scheme of a STM-setup. Note that during the experiments the tip is partially immersed in the fluid layer. (B) Scheme of the SNOM-setup. IF = interference filter, BC = Berek's compensator, OFC = optical fiber coupler, OF = optical fiber, PD = photodiode, F = filter, KM = kinematic mirror, BS = beam splitter, CCD = charge coupled device, APD = avalanche photodiode, OMA = optical multichannel analyser.

The high-resolution qualities of these techniques in addition to their local probing character make them very useful tools for the study of surface phenomena in various research fields. In our research group these techniques have been used to study several photo-induced processes at surfaces. In the first section here we will demonstrate how SNOM is useful in characterising and modifying the optical properties of materials on a sub-micrometer size. In the second, we will exemplify the use of STM for studying photo-induced reactions at the liquid/solid interface.

Scanning near-field optical microscopy

There are a number of excellent reviews on SNOM,[8–12] and its applications in the study of organic materials.[11,13–16] The reader is referred to these reports for detailed information on the technique and some of its applications. We focus on some of our results on the use of SNOM for the study of organic fluorescent materials and photo-induced local modifications in thin films or on substrates.

Single objects

Latex beads

As stated in the introduction, SNOM allows study of the optical properties of materials with subwavelength resolution. Thin poly(vinyl alcohol) (PVA) polymer films containing dye-labelled 100 nm beads were investigated.[17,18]

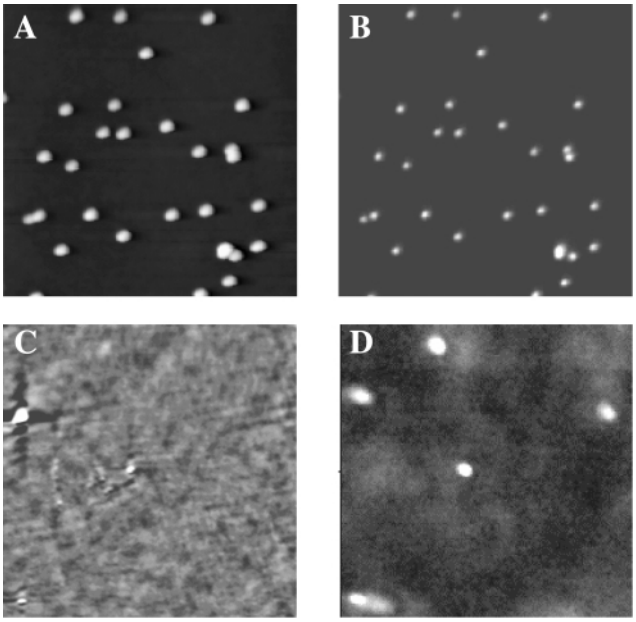

Fig. 2 SNOM image sets taken from a *ca*. 50 nm thin film (A topography, B fluorescence) and a *ca*. 10 μm thick film (C topography, D fluorescence) consisting of *ca*. 100 nm dye-labeled latex particles embedded in a PVA matrix. Image sizes: $10 \times 10\ \mu m^2$. The excitation wavelength is 488 nm for set A, B and 458 nm for set C, D.

Fig. 2 comprises a topographic (A) and a fluorescence map (B) of a thin polymer film (*ca*. 50 nm as measured by AFM) consisting of dye-labelled latex particles embedded in a PVA matrix. The image set was acquired while the polymer film was irradiated through the aperture probe at an excitation wavelength of 488 nm.[18] Based on their measured size the bead-like structures in the topography images can be attributed to single latex particles. The pattern of the black–white contrast in the topographic images corresponds to a diameter of 109 nm. In the fluorescence map in Fig. 2B, the particles displayed in the topographic image can be correlated with distinct spots of a fluorescence intensity exceeding the background intensity. Note that the size of the fluorescence spots is substantially smaller than the features in the topography image. In the latter, the signal is derived from the interaction of the tip end (including the Al coating surrounding the aperture) and the sample surface, while for the fluorescence measurement, the dimension of the aperture itself determines the optical resolution. The latex particles were also embedded in a film a few μm thick.[17] Fig. 2C,D shows one image set representing on the left side the topography and on the right side the fluorescence map. Where the topography shows only structures with a height substantially less than the size of a latex particle, fluorescence spots of high intensity appear in the fluorescence maps. Only some of these spots correlate with the topographic information. This finding reveals a unique capability of SNOM. In contrast to most scanning probe microscopies, SNOM is able to probe subinterface properties occurring in spatial domains that are located a few 10 nm beneath a sample–air interface. The luminescence properties of these domains can be addressed by the collimated radiation field generated by the aperture probe.

In order to gain insight in the distribution of functional groups and the distance between these functional groups in latex beads, energy transfer in latex beads has been investigated. Therefore, the shell of latex beads (core = polystyrene, shell = poly(acrylate) (PA), diameter *ca*. 100 nm) has been covalently labelled with two different dyes, Bodipy and TMR (Fig. 3). The beads are dispersed in a 10 nm thin PVA matrix. The spectral overlap between the emission spectrum of Bodipy (energy donor) and the absorption spectrum of TMR (energy acceptor) allows for efficient energy transfer between those dyes within individual latex beads. The energy transfer process has been 'visualized' by recording the wavelength dependent fluorescence intensity of individual beads obtained upon excitation of the Bodipy chromophores for different label concentrations. The fluorescence maps and spectra clearly show efficient excitation energy transfer within a single latex bead and energy transfer is more pronounced when the relative distances between donor and acceptor decrease. The efficiency of the energy transfer ranges from 85 to 57%, depending on the dye concentration (Fig. 3A). No significant differences have been found between different beads. When those beads are dispersed in a poly(acrylate) matrix, which has a lower T_g compared to PVA, the excitation energy transfer efficiency decreases (74% relative to 85%) and this is more pronounced (62%) when the samples are annealed (Fig. 3B). This has been attributed to 'swelling' of the PA latex shell, resulting in an increase of the distance between chromophores and a decrease in energy transfer efficiency.

SNOM not only allows investigation of photophysical properties of chromophore labelled latex beads, but also permits the visualization of a phototransformation leading to bleaching.[17] The latex particles in the topographic image of Fig. 4A are clearly correlated with fluorescence structures in the corresponding fluorescence map (Fig. 4B). The torus-like shaped fluorescence structures do not directly reflect the dye distribution on the particles, but result from the overlap of the intensity distribution of the radiation field beneath the aperture. In the course of the photobleaching experiment, the SNOM probe was positioned above the particle on the right, and the particle was raster-scanned while the particle was irradiated with the 458 nm light emanating from the probe. After 2 h, almost no fluorescence is observed from the denoted position in the fluorescence map (Fig. 4D), where the probe illuminated the latex particle. However, the topography image (Fig. 4C) indicates that the particle was not removed or destroyed during scanning. This experiment demonstrates that a photochemical reaction can be induced upon irradiation with the SNOM probe and that the photochemical reaction induced by the optical near-field is restricted to a nanometer length scale. Local photobleaching has also been demonstrated in molecular systems,[19] supramolecular systems[20] and polymers.[21]

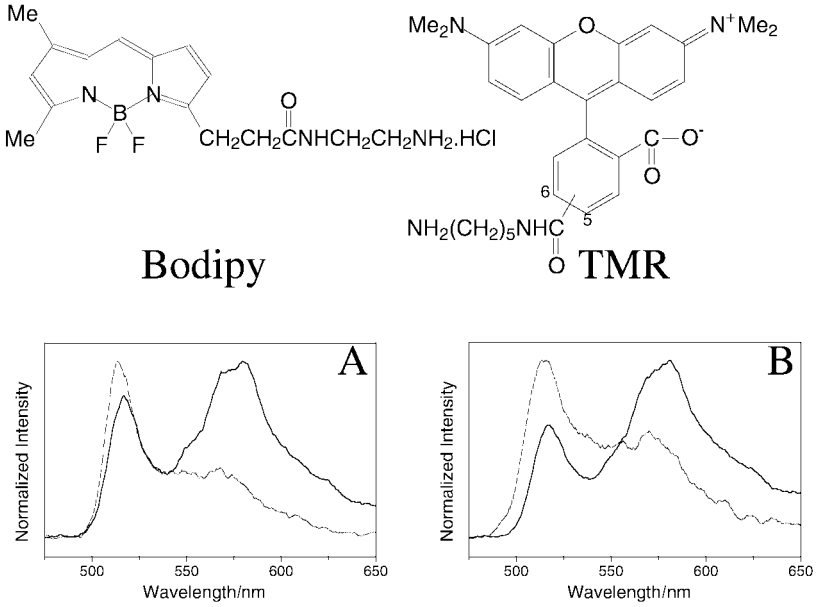

Fig. 3 Chemical structures of Bodipy [λ_{max}(em) = 514 nm] and TMR [λ_{max}(em) = 572 nm]. Normalized fluorescence spectra obtained on single beads. (A) High (black) and low (gray) label concentrations of Bodipy/TMR. The polymer film is PVA. (B) Beads with high label concentration dispersed in PVA-matrix (black) and PA-matrix (gray). The excitation wavelength is 458 nm.

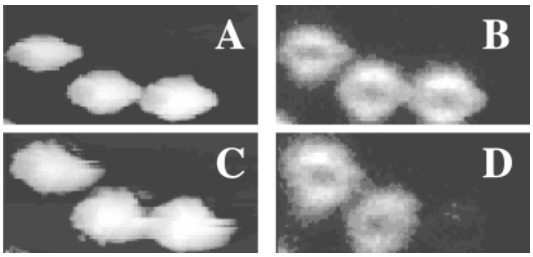

Fig. 4 SNOM image sets comprising the topographic images (A, C) and the fluorescence maps (B, D) of a section of a thin film, before and after photobleaching the right latex bead, respectively.

Supramolecular structures

Porphyrin rings

In addition to the study of single objects, SNOM also helps to visualize parts of supramolecular structures. The formation of ring-like structures has been observed in the evaporation process of organic solutions containing a broad range of materials including metal particles,[22] polymers,[23] proteins[24] and organic molecules.[25–27] In particular, the deposition of these solutions on a substrate lead to micron scale ring-shaped arrangements of the solute/dispersed materials. Using SNOM, a deeper insight into the morphology and the local optical properties of solvent-evaporated porphyrin thin films has been reached. In particular, the effects of the concentration of the starting solution on the film morphology have been investigated.

Evaporation of a 10^{-6} M solution of PtP (Fig. 5A) in $CHCl_3$ on glass yielded symmetric rings for which the topography and fluorescence images are highly correlated.[25]

The ring diameter ranges between 100 nm and 10 μm, while the height of the rims, determined from the SNOM topographic image, varies between 10 and 300 nm. The fluorescence intensity measured inside the rings equalled the background value indicating the absence of porphyrin material at these positions. The use of a more dilute solution (10^{-7} M) resulted in the formation of incomplete ring-shaped assemblies that were made up from individual isolated structures which were observed both in the topography and the fluorescence image (Fig. 6B). In these conditions the rings had smaller diameters and the heights of the beads that comprise most of the rings were substantially smaller than the heights of the well formed rings prepared from more concentrated solutions.

A further characterization of the films in terms of the local optical properties and molecular organization was performed using fluorescence polarization imaging. From these data it

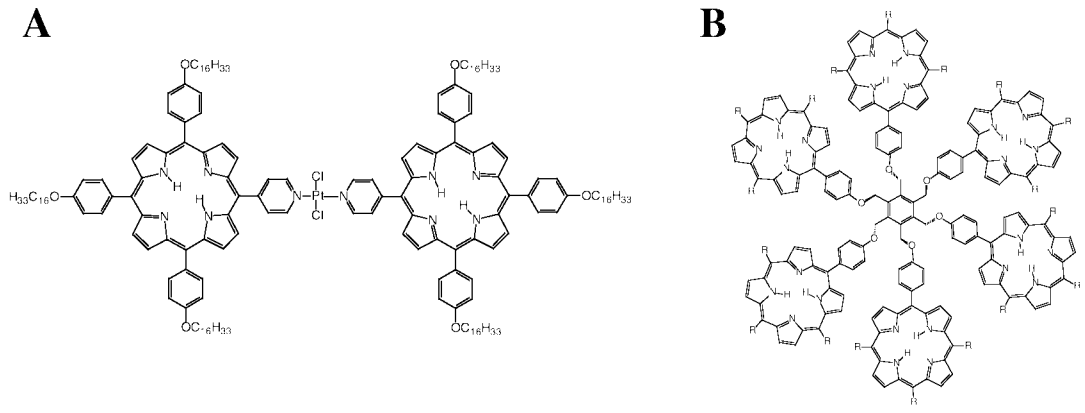

Fig. 5 Schematic representation of PtP (A) and BP_6 (B).

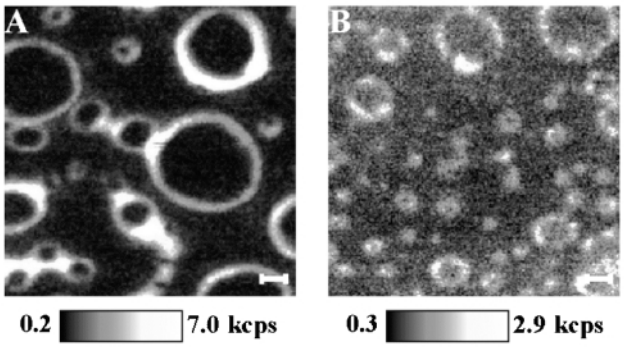

Fig. 6 SNOM fluorescence images of evaporated films of PtP/$CHCl_3$ solutions on glass. The scale bars represent 1 μm. (A, B) Fluorescence image taken on a sample prepared by solvent casting of a 10^{-6} M (A), and a 10^{-7} M (B) solution.

could be stated that in these films small, organized aggregates are present which, by using linearly polarized light for excitation, can be photoselected and that these aggregates show polarized emission. The length of these aggregates, as determined from the line profiles taken in the fluorescence polarization images, varies between 50 nm and *ca.* 300 nm. Annealing of the PtP ring samples leads to an increase in size, density and ordering of the aggregates.

Similar experiments were performed using samples prepared by evaporation of a $BP_6/CHCl_3$ (Fig. 5B) solution. For the samples studied before annealing, the images corresponding to the different polarization configuration were identical (images are not presented). On the other hand, the annealed samples exhibit strong polarization contrast. When the fluorescence intensity distributions in the rings are compared to what was found for PtP, a much smoother profile is observed. For the BP_6 samples the intensity distribution depends over a longer range on the excitation polarization with parallel emission polarization. When the excitation polarization is oriented horizontally in the image (Fig. 7B) the upper and lower parts of the rings have a relative higher intensity than the left and the right parts of the rings. Turning the excitation polarization 90 degrees (Fig. 7C) results in higher fluorescence intensity for the left and right parts of the ring. The different intensity distributions are not observed in the images taken with the excitation and the emission polarization oriented perpendicular with respect to each other. The observed fluorescence pattern can only be explained if there is a preferential orientation of the molecules in the rings. This would lead to a specific orientation of the absorption dipoles in the ring. Using polarized excitation results in a preferential absorption of the excitation light at the positions where the polarization and the absorption dipole of the chromophore are parallel. This results in higher fluorescence intensity at the respective positions. If the molecules are schematically presented as disks the orientation should be preferentially perpendicular to the sample plane. A possible arrangement of the disks in the rings could be one with the planes parallel or perpendicular to the radial of the ring.

These rings have been mechanically manipulated at the submicron scale with AFM. This manipulation was carried out by implementing an interface, called the nanoManipulator, on a combined AFM–confocal microscope.[28] A small amount of the fluorescent material from the ring could be displaced with the AFM tip. A special tool (sweep mode), in which the AFM tip is moved very fast perpendicular to the direction of the desired manipulation which creates a virtually broader tip, allowed a modification of 130 nm (Fig. 8A). The resolution attainable in these kinds of experiments could go down below 100 nm and is primarily determined by the tip and sample geometry. Besides the possibility of mechanically manipulating porphyrin rings using the force applied by an AFM tip, it is feasible to manipulate or modify locally the optical properties of these rings in terms of tip-induced photobleaching using the light coming from a SNOM-tip.[28] In such an experiment the dimensions of the manipulated area are related to the size of the SNOM probe used in the experiment (Fig. 8B).

J-Aggregates in polyelectrolyte layers

As an alternative to Langmuir–Blodgett (LB) film deposition,[29,30] self-assembly techniques based on covalent or coordination chemistry were developed.[31,32] In the beginning of the 1990s, Decher *et al.* demonstrated the alternate adsorption of cationic and anionic polyelectrolytes as a novel technique for the preparation of molecular multilayers.[33] This method was applied for the layer by layer fabrication of alternate assemblies containing J-aggregates[34,35] of a cyanine dye. J-Aggregates act as a multi-charged supramolecular ensemble, which promises a strong adsorption. Only a few papers report local properties of J-aggregates on a nanometer scale. The group of Barbara has applied SNOM to the investigation of J-aggregates, examining J-aggregates of 1,1′-diethyl-2,2′-cyanine iodide, pseudoisocyanine (PIC) which were formed in a solution with poly(vinyl sulfate) (PVS) and spin-coated onto quartz substrates.[20,36,37]

We have used SNOM for the investigation of J-aggregates of 3,3-disulfopropyl-5,5′-dichloro-9-ethylthiacarbocyanine (THIATS), formed in a layer by layer self-assembled multilayer when alternating with the cationic polyelectrolyte, poly-(allylamine) (PAH) The influence of the top layer and of ageing of the samples was studied.

Fluorescence images were obtained for a freshly deposited sample [glass/poly(styrene sulfonate] (PSS)/PAH/THIATS/PAH). The micrographs were obtained by excitation at 514 nm and collecting the total fluorescence. In the fluorescence micrograph, very short organized structures with an enhanced

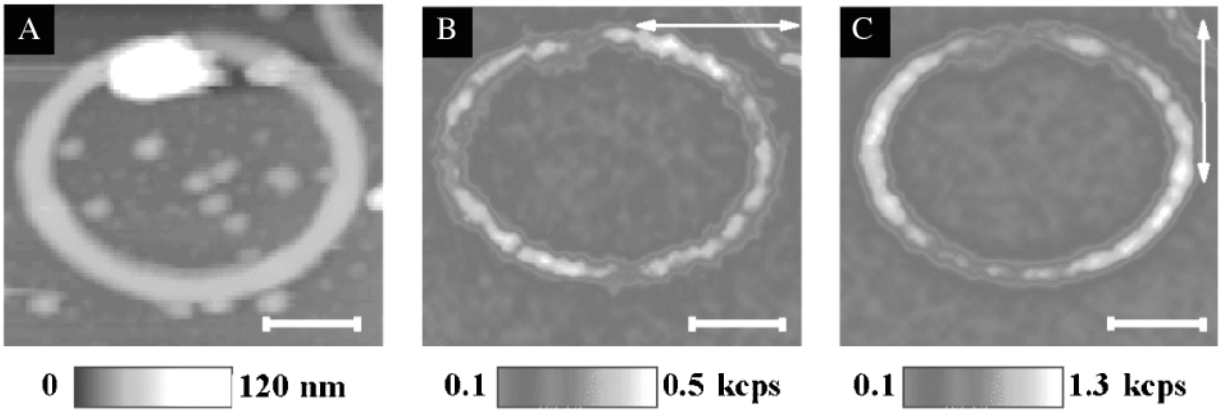

Fig. 7 A set of SNOM topographic and fluorescence polarization images acquired from a sample prepared by evaporation of a 10^{-6} M $BP_6/CHCl_3$ solution on glass after annealing in an oven at 75 °C for several days. The white scale bar on each image represents 1 μm. The orientation of the excitation polarization is indicated with the white arrows on the images. All fluorescence images are acquired with a parallel polarization configuration.

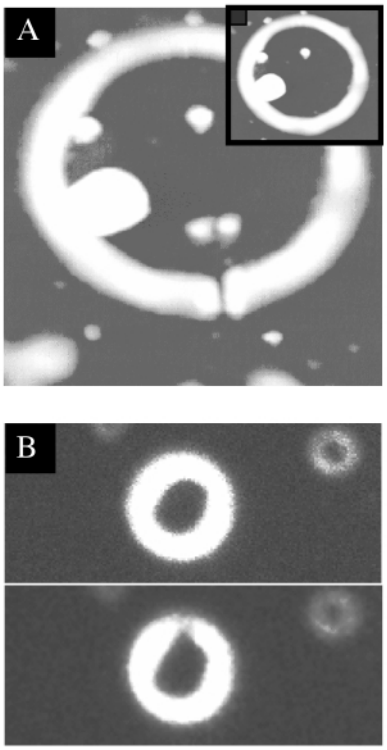

Fig. 8 (A) Mechanical and (B) optical manipulation of porphyrin rings at the submicrometer scale. (A) AFM image. The modification (cut through the ring) is around 130 nm. The insert is the intact ring before manipulation. (B) SNOM fluorescence images of a porphyrin ring before (upper half) and after (lower half) local photobleaching with a SNOM tip, leading to a modification of 280 nm wide.

fluorescence can be observed (Fig. 9A). Annealing of this sample at 70 °C induced structures in the fluorescence micrograph which resemble a needle-like pattern (Fig. 9B). The structures in the freshly deposited sample can be the nucleating sites for this pattern. The needle-like pattern was also observed in the fluorescence micrographs obtained for a multilayer which was kept at room temperature for 45 days after deposition (Fig. 9C). This suggests that a re-orientation and redistribution of the dye molecules into microcrystals does not happen immediately after deposition but that ageing of the sample is needed to obtain the needle-like pattern in the fluorescence micrograph. High-resolution images (not shown) reveal that the experimental width of the needles, measured in near-field, is about 80 nm, which corresponds to the lateral optical resolution of the experiment. The length of the needles exceeds a micron. We attribute the formation of needle-like structures to the PAH layer on top of the dye layer which must induce a redistribution and re-orientation of the dye molecules into microcrystals. The smoothness of topography suggests that the height of the microcrystals is small compared to the thickness of one polymer layer.[38,39]

In order to investigate to what extent the crystallites observed in the fluorescence image are oriented, polarized fluorescence images were obtained. Fig. 10 displays fluorescence images for a sample with PAH as top layer and for which the time between the deposition and the measurements was 45 days. Image 10A, B, C and D are the micrographs with 0°–0°, 0°–90°, 90°–0°, 90°–90° orientation of the polarizer and analyser, respectively. For different orientations of the emission polarizers different image contrasts were obtained. Fluorescence micrographs, obtained with the same orientation of the analyser but with different orientations of the polarizer, show the same fluorescent structures. The image contrast is furthermore independent of the excitation polarization at a fixed emission polarization. This indicates that the absorbing species is oriented randomly and that no photoselection occurs. One should realise that 514 nm, where the excitation occurs, is far from the absorption maximum of the J-aggregates situated at 623 nm. At 514 nm absorption is probably mainly due to residual monomers and sandwich dimers which transfer their excitation energy to the J-aggregates.

With a 'horizontal' orientation of the analyser, the emission of 'vertically' oriented needles was enhanced, while with a 'vertical' orientation of the analyser, the emission of 'horizon-

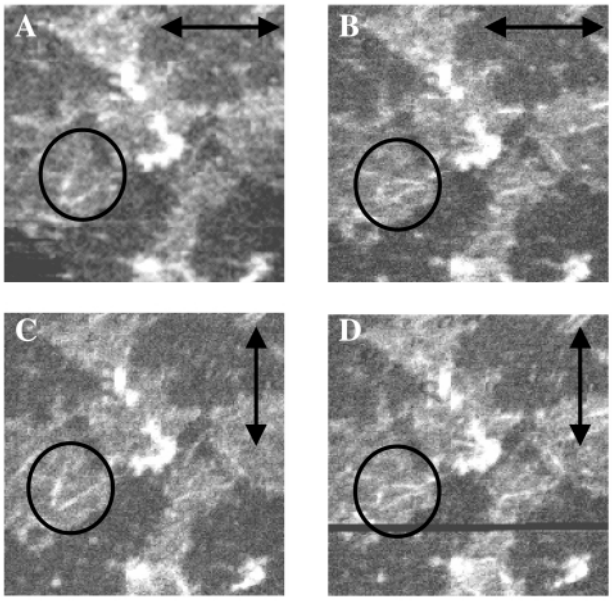

Fig. 10 Polarized SNOM measurements of a THIATS-containing multilayer covered by a layer of poly(allylamine) (PAH): Fluorescence micrographs with 0°–0° (A), 0°–90° (B), 90°–0° (C), 90°–90° (D) orientation of the excitation polarizer and fluorescence emission analyser respectively. The arrows indicate the excitation polarization. Excitation occurred at 514 nm.

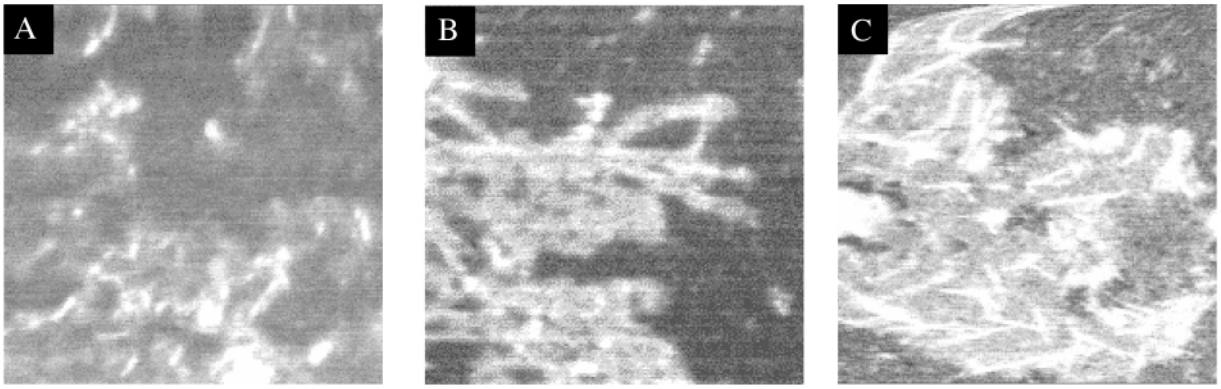

Fig. 9 SNOM fluorescence micrographs of a 10 μm × 10 μm sample with a PAH top layer: fresh sample (A), annealed sample (B), aged sample (C). Bright areas correspond to high fluorescence while dark areas correspond to low fluorescence relatively to each other.

tally' oriented needles was enhanced. This indicates that the transition dipoles of the emitting species have an orientation, which is highly correlated over several hundreds of nanometers to several microns. Furthermore in the 'horizontally' oriented needles, the emission dipole of the dye molecules will be oriented preferentially 'vertical' and *vice versa*. Needle-like structures, which are oriented at an angle of 45°, are visible in all the fluorescence micrographs. In Fig. 10, the area where the influence of the polarizers is clearly visible is marked with a white circle.

Excitation of residual monomers and dimers at 514 nm resulted in J-aggregate emission, which is polarized. The emission dipole of the dye molecules is oriented perpendicular to the needles. If a 2-D brickstone arrangement[40,41] is assumed for the aggregates their maximum π–π-interactions will occur perpendicular to the transition dipole and in the plane of the aggregate. Also the largest plane of the molecule is that parallel to both the long and the short axis. Hence packing along this plane will both be characterized by the largest π–π-interactions and reduce the hydrophobic interaction to a maximal extent. Therefore, the maximum growth rate of the microcrystals will be observed in those directions.

Scanning tunnelling microscopy and photochemistry

Where optical detection with SNOM is still limited to tens of nm, STM allows us to increase further the spatial resolution. In the last two decades, STM has proven to be a very valuable tool for the structure determination of surfaces at subnanometer resolution. The use of this technique is not restricted to a low temperature UHV environment but it has a wider application field and has also been applied successfully under ambient conditions and even in liquids. Moreover, the use of STM has been extended to the study of organic molecules physisorbed on conductive substrates at the liquid/solid interface.[42–47] In our research group, topics such as structure,[48] chirality,[49–51] dynamics[52–56] and light-induced reactions[57–59] are studied in physisorbed organic monolayers at the liquid/solid interface under ambient conditions.[60] The samples are prepared by applying a drop of a solution containing the compound under investigation on the basal plane of a freshly cleaved piece of highly oriented pyrolytic graphite (HOPG). The molecules are adsorbed on the graphite surface by physisorption. Adsorbate–substrate and adsorbate–adsorbate interactions lower the molecular mobility. This decrease in mobility (dynamics) is important for successful high resolution imaging with STM, which is often realized, in our group, by using molecules which display high affinity for the graphite substrate, for instance by having long alkyl chains. Intermolecular hydrogen bonding stabilises the two-dimensional network formed by the physisorbed molecules studied. In contrast to Langmuir–Blodgett films of fatty acids and their salts, the molecules are in most cases oriented parallel to the graphite substrate. It is important to note that during the measurements, the STM tip is immersed in the solution on top of the monolayer and that during the measurement molecules in the physisorbed monolayer might undergo desorption–adsorption dynamics. The presence of the solvent layer has some advantages. On one hand, it allows for the repair of defects in the monolayer by the desorption–adsorption dynamics and on the other hand, it lowers the force of the STM tip on the monolayer during scanning.

Using this experimental approach, we have investigated some photochemical reactions at the liquid/graphite interface. The aim of these studies was to demonstrate the feasibility of using STM for the study of photo-induced processes and on the other hand to learn more about these processes by STM.

A reversible reaction: *trans–cis* isomerization

With the aim of imaging the starting material and the reaction product of a reversible photoreaction, the *cis–trans* isomerization of an azo isophthalic acid derivative was investigated.[58] Upon irradiation with light of an appropriate wavelength, the *trans* to *cis* isomerization can be induced.

To achieve an efficient conversion of the *trans* to the *cis* isomer, the irradiation wavelength should match the absorption maximum of the *trans* isomer. The absorption maximum of the *cis* and *trans* isomer is situated at 317 and 360 nm, respectively. Upon irradiation at 366 nm, a photostationary mixture with a high *cis* isomer content is reached. When kept in the dark at room temperature the *cis* isomer spontaneously converts to the thermodynamically more stable *trans* isomer. For the STM experiments, an almost saturated solution of the azo compound in undecan-1-ol was applied on the surface of a freshly cleaved HOPG piece (Fig. 11). The solvent undecan-1-ol was selected

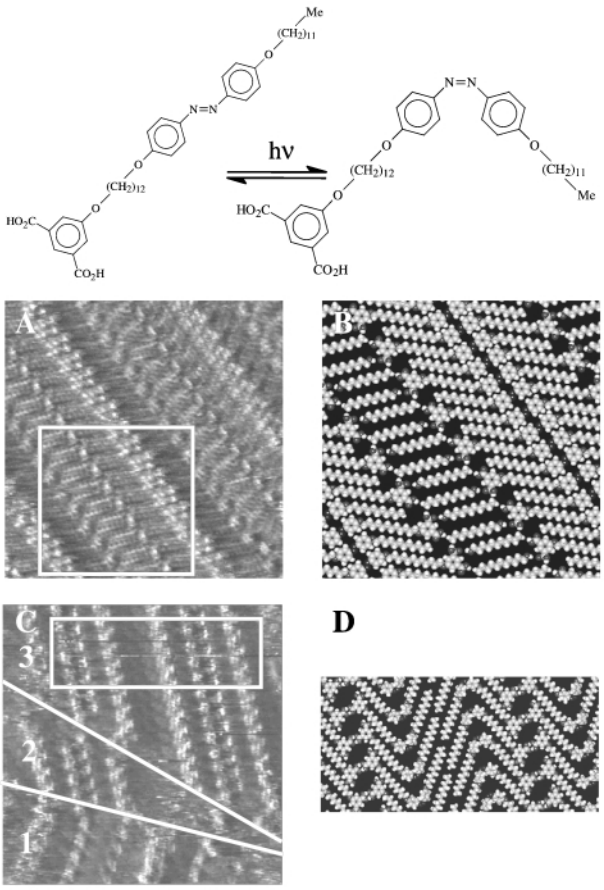

Fig. 11 *Cis* and *trans* isomer, reagent and product of a reversible photo-induced reaction. (A) STM image of an ordered monolayer of *trans* formed by physisorption from undecan-1-ol. Image size is 13 × 13 nm². White corresponds to the highest and black to the lowest measured tunnelling current in the image. (B) Molecular model for the two-dimensional packing of *trans*. The molecular model represents the area indicated in the STM image. (C) After illumination, STM image of an ordered monolayer of coexisting *cis*- and *trans*-domains. The domain boundaries are indicated by white lines. Image size is 13.4 × 13.4 nm². The molecular order in domain 1 corresponds to *trans*. The molecular order in domain 2 and 3 can be correlated with *cis*.

for its high boiling point (the solvent layer stays on top of the monolayer for several hours); in addition the solvent competes for intermolecular hydrogen bonding of the solute molecules which might disfavour physisorption.

Fig. 11A and 11B show an STM image and model of a monomolecular layer of the *trans*-form physisorbed from undecan-1-ol and shielded from light. The images are recorded in the constant height mode and the contrast is a function of the tunnelling probability as a function of *xy* coordinates. Bright and dark features in the images reflect a high and low tunnelling probability, respectively. Distinct bright spots corresponding to the isophthalic acid groups are easily recognized in the image. The somewhat broader bright bands represent the azobenzene moieties; in addition, the alkyl chains can be recognized in the image. Undecan-1-ol molecules are co-deposited in lamellae

separating lamellae of the azo-compound. Fig. 11C shows an STM image of a monolayer obtained by physisorption from a photostationary mixture after illumination of the solution in a cuvette (*ex situ*) at 366 nm. In addition to the regular monolayer structure characteristic for *trans* (domain 1), a new monolayer structure appeared which was not observed for *trans* monolayers (domains 2 and 3). Therefore, the patterns observed in these two domains must originate from a different molecular arrangement. Again, the bright spots correspond to the isophthalic acid groups and the broader bright bands to the azobenzene moieties. The measured lamellar distances and the observed molecular packing correspond to a monolayer of self-assembled *cis* isomers without solvent co-deposition. The absence of solvent co-deposition is probably due to the spatial orientation of the acid functions in the molecular arrangement of the *cis* isomer. It was not possible to form adlayers, which show solely *cis* structure. This can be attributed to the photostationary character of the mixture and to the larger affinity of *trans* compared to *cis* to form monolayers on the graphite surface. During imaging, the *cis* domains disappear with time. Finally, only *trans* domains could be observed, illustrating the reversibility of the reaction at the liquid/graphite interface. Similarly, *trans–cis* isomerization could be induced and their respective domains imaged by irradiating *in situ* a droplet of the *trans* isomer dissolved in undecan-1-ol directly on the graphite surface.

A possible mechanism for replacement of physisorbed 'reactant' molecules by the 'product' initiated by *in situ* illumination is the following. Irradiation of the system will lead to a change of the equilibrium composition and a concentration gradient in the supernatant solution. A decrease in *trans* concentration will induce desorption and enhance the adsorption of *cis* molecules. In addition, the isomerization reaction could also occur on the graphite surface itself and initiate the *cis*-product domain formation although this is expected to contribute only to a minor extent due to steric hindrance. During imaging (illumination off), these *cis* domains disappear with time until finally only *trans* isomer domains remain, due to the thermal back reaction (*cis* to *trans*).

The *cis–trans* isomerization has also been studied for another isophthalic acid derivative where one of the phenyl groups of the azobenzene moiety is the isophthalic acid group. Also for this compound the reaction could be visualized, however only after illumination *ex situ*.[60]

An irreversible reaction

In addition to a reversible *cis–trans* isomerization, an irreversible photoreaction was studied: the phototransformation of 10-diazo-2-hexadecylanthrone to 2-hexadecyl-9,10-anthraquinone.[57] Irradiation leads to the dissolution of the highly ordered molecular pattern of the reactant, starting at a domain boundary. When the irradiation is stopped, the highly ordered pattern reappeared and recrystallization of the reactant molecules occurred. As described in the previous section, the desorption must be the result of the formation of a concentration gradient induced by illumination. When irradiation is stopped, the system relaxes and the 2D crystal is reformed. Only when all reactant was transformed to product, which occurred after several illumination cycles were monolayers of 2-hexadecyl-9,10-antraquinone formed. Both phototransformations are believed to take place predominantly in the supernatant solution.

A topochemical reaction

To demonstrate the possibility of reactivity *within* the physisorbed monolayer, the study of a topological reaction was considered: the photopolymerization of a diacetylene[59] for which it is known that the relative orientation of the diacetylene monomer groups is critical as is shown in numerous studies in 3D crystals. The molecule chosen in this study is the diacetylene containing isophthalic acid derivative (Fig. 12).

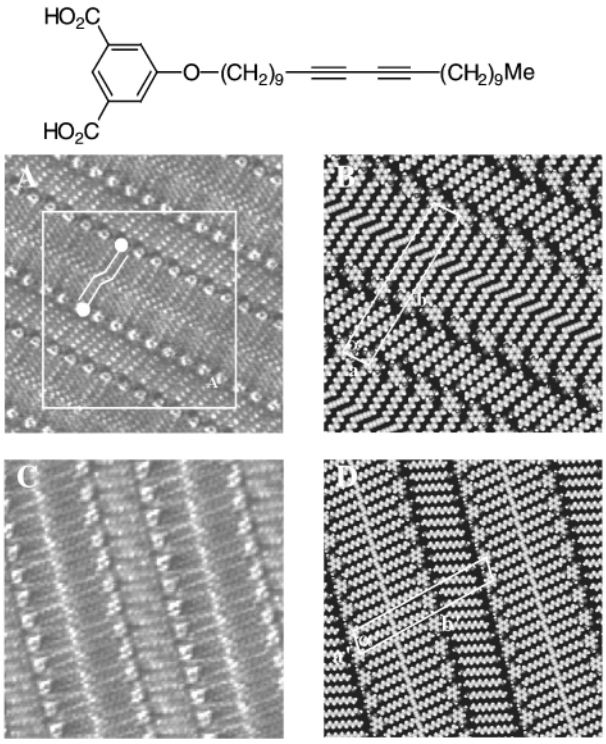

Fig. 12 Molecular structure of 5-(10,12-tricosadiinyloxy)isophthalic acid. (A) STM image of a physisorbed monolayer monomer from a solution in undecan-1-ol. Image size is 12.7 × 12.7 nm². The orientation of two molecules is indicated with a stick model. (B) Corresponding molecular model of the area indicated in the STM image in (A). (C) STM image of a polymerized monolayer structure. Image size is 10.8 × 10.8 nm². (D) Molecular model of the imaged area in (C).

This compound forms a physisorbed monolayer spontaneously at the liquid/graphite interface from a undecan-1-ol solution (Fig. 12A). The structure consists of lamellae of the diacetylene derivative alternated by solvent lamellae. The diacetylene moieties appear as bright spots in the middle of the lamellae. Within a lamella, the distance between isophthalic acid groups is 9.44 ± 0.09 Å. The alkyl chains are lying parallel to the substrate in the direction of one of the main graphite axes, and the orientation is modelled in Fig. 12B. After *in situ* illumination (254 nm, no scanning) of the monolayer film on graphite, the surface was re-examined, using the same scanning parameters as prior to the illumination, and again monolayer structures are observed (Fig. 12C). Isophthalic acid groups and solvent molecules are well resolved. The contrast in the middle of a lamella can be described by a series of bright spots, clearly distinct from the individual acetylene units, which suggests that the monolayer structure might be polymerized along the lamella direction. The most important change in the monolayer structure, however, is the change in spacing between the isophthalic acid groups. The distance was determined to be 9.81 ± 0.05 Å, in contrast to the unpolymerized repeating distance of 9.44 ± 0.09 Å. A molecular model for a polymerized monolayer structure is shown in Fig. 12D. The experimental value of 9.81 Å for the isophthalic acid group distance is in perfect accordance with the value of 9.82 Å obtained in a model optimized for the polymer chain. Consequently, the repeating distance in the polymer backbone is 4.91 Å which is in agreement with the three-dimensional crystal structure data of polymerized diacetylenes.[61] The structural parameters, describing the orientation of adjacent diacetylene units in unpolymerized monolayers, correspond to those values for which it was shown experimentally by X-ray crystallography of 3-D samples that crystallized diacetylene monomers could polymerize.[61]

Conclusions

The invention and development of scanning probe microscopy techniques has opened new ways to study surface phenomena with unprecedented resolution. The strength of these techniques is the very local nature of the probing mode and their general applicability even under ambient conditions, combined with the very high resolution. Both STM and SNOM have proven to be valuable tools in the study of thin organic films and photo-induced modifications on a very small scale. STM is for these kinds of systems used for the observation of the reactions while SNOM can optically modify material in an active way. Both techniques will continue to contribute in an important way to the study of photo-induced modifications on surfaces.

Acknowledgements

We thank the DWTC, through IUAP-IV-11, the F.W.O.-Vlaanderen and ESF SMARTON for financial support. We also gratefully thank Dr K. Grim, Dr P. Vanoppen, Dr K. Jeuris, A. Gesquière, M. Abdel-Mottaleb, E. Rousseau and P. Foubert for their substantial input in the realization of the experiments. S.D.F. and J.H. thank the Fund for Scientific Research–Flanders (FWO) for a postdoctoral fellowship. The collaborations were made possible thanks to the TMR project SISITOMAS.

Notes and references

1 G. Binnig and H. Rohrer, *Helv. Phys. Acta*, 1982, **55**, 726.
2 U. Dürig and D. W. Pohl, *J. Appl. Phys.*, 1986, **59**, 3318.
3 E. Betzig, A. Lewis, A. Harootunian, M. Isaacson and E. Kratschmer, *Biophys. J.*, 1986, **49**, 269.
4 H. J. Dai, J. H. Hafner, A. G. Rinzler, D. T. Colbert and R. E. Smalley, *Nature*, 1996, **384**, 147.
5 S. S. Wong, E. Joselevich, A. T. Woolley, C. L. Cheung and C. M. Lieber, *Nature*, 1998, **394**, 52.
6 E. Betzig and R. J. Chichester, *Science*, 1993, **262**, 1422.
7 J. A. Veerman, M. F. Garcia-Parajo, L. Kuipers and N. F. van Hulst, *J. Microsc.-Oxford*, 1999, **197**, 477.
8 E. Betzig and J. K. Trautman, *Science*, 1992, **257**, 189.
9 H. Heinzelmann and D. W. Pohl, *Appl. Phys. A.*, 1994, **59**, 89.
10 D. Courjon and C. Banier, *Rep. Prog. Phys.*, 1994, **57**, 989.
11 R. C. Dunn, *Chem. Rev.*, 1999, **99**, 2891.
12 B. Hecht, B. Sick, U. P. Wild, V. Deckert, R. Zenobi, O. J. F. Martin and D. W. Pohl, *J. Chem. Phys.*, 2000, **112**, 7761.
13 D. A. Vanden Bout, J. Kerimo, D. A. Higgins and P. F. Barbara, *Acc. Chem. Res.*, 1997, **30**, 204.
14 P. F. Barbara, D. M. Adams and D. B. O'Connor, *Annu. Rev. Mater. Sci.*, 1999, **29**, 433.
15 P. Zhang, R. Kopelman and W. Tan, *Solid State Mater. Sci.*, 2000, **25**, 89.
16 R. Zenobi and V. Deckert, *Angew. Chem., Int. Ed.*, 2000, **39**, 1746.
17 M. Rücker, P. Vanoppen, F. C. De Schryver, J. J. Ter Horst, J. Hotta and H. Masuhara, *Macromolecules*, 1995, **28**, 7530.
18 K. Jeuris, P. Vanoppen, F. C. De Schryver, J. W. Hofstraat, L. G. J. van der Ven and J. W. van de Velde, *Macromolecules*, 1998, **31**, 8579.
19 A. K. Kirsch, V. Subramaniam, A. Jenei and T. M. Jovin, *J. Microsc.*, 1999, **194**, 448.
20 D. A. Higgens and P. F. Barbara, *J. Phys. Chem.*, 1995, **99**, 3.
21 J. A. DeAro, R. Gupta, A. J. Heeger and S. K. Buratto, *Synth. Met.*, 1999, **102**, 865.
22 P. C. Ohara, J. R. Heath and W. M. Gelbaert, *Langmuir*, 1998, **14**, 3418.
23 L. Zhou, P. C. Zhang, P. K. H. Ho, G. Q. Xu, S. F. Y. Li and L. Chan, *J. Mater. Sci. Lett.*, 1996, **15**, 2080.
24 U. Thiele, K. Mertig and W. Pompe, *Phys. Rev. Lett.*, 1998, **80**, 2869.
25 J. van Esch, M. F. Roks and R. J. M. Nolte, *J. Am. Chem. Soc.*, 1986, **108**, 6093; A. P. H. J. Schenning, D. H. W. Hubert, M. C. Feiters and R. J. M. Nolte, *Angew. Chem., Int. Ed. Engl.*, 1994, **23**/**24**, 2468.
26 J. Hofkens, L. Latterini, H. Faes, P. Vanoppen, K. Jeuris, S. De Feyter, J. Kerimo, P. F. Barbara, F. C. De Schryver, A. E. Rowan and R. J. M. Nolte, *J. Phys. Chem.*, 1997, **49**, 10 558.
27 H. A. M. Biemans, A. E. Rowan, A. Verhoeven, P. Vanoppen, L. Latterini, J. Foekema, A. P. H. J. Schenning, E. W. Meijer, F. C. De Schryver and R. J. M. Nolte, *J. Am. Chem. Soc.*, 1998, **120**, 11 054.
28 P. Foubert, P. Vanoppen, M. Martin, T. Gensch, J. Hofkens, A. Helser, A. Seeger, R. M. Taylor, A. E. Rowan, R. J. M. Nolte and F. C. De Schryver, *Nanotechnology*, 2000, **11**, 16.
29 I. Langmuir, *J. Am. Chem. Soc.*, 1917, **39**, 1848.
30 K. B. Blodgett, *J. Am. Chem. Soc.*, 1935, **57**, 1007.
31 L. Netzer and J. Sagiv, *J. Am. Chem. Soc.*, 1983, **105**, 647.
32 G. Cao, H. G. Hong and T. E. Mallouk, *Acc. Chem. Res.*, 1992, **25**, 420.
33 G. Decher, J. D. Hong and J. Schmitt, *Thin Solid Films*, 1992, **210**/**211**, 831.
34 G. Scheibe, *Angew. Chem.*, 1939, **52**, 633.
35 E. E. Jelley, *Nature*, 1936, **138**, 1009.
36 D. A. Higgins, P. J. Reid and P. F. Barbara, *J. Phys. Chem.*, 1996, **100**, 1174.
37 D. A. Higgins, J. Kerimo, D. A. Vanden Bout and P. F. Barbara, *J. Am. Chem. Soc.*, 1996, **118**, 4049.
38 G. Decher and J. Schmitt, *Prog. Colloid Polym. Sci.*, 1992, **89**, 160.
39 M. Lösche, J. Schmitt, G. Decher, W. G. Bouwman and K. Kjaer, *Macromolecules*, 1998, **31**, 8893.
40 V. Czikkely, H. D. Forsterling and H. Kuhn, *Chem. Phys. Lett.*, 1970, **6**, 11.
41 H. Asanumo, K. Ogawa, H. Fukunaga, T. Tani and J. Tanaka, *Proceedings ICPS '98: International Congress on Imaging Science*, University of Antwerp: Belgium, 1998.
42 J. S. Foster and J. E. Frommer, *Nature*, 1988, **333**, 542.
43 G. C. McGonigal, G. C. Bernhardt and D. J. Thomson, *Appl. Phys. Lett.*, 1990, **57**, 28.
44 J. P. Rabe and S. Buchholz, *Science*, 1991, **253**, 424.
45 J. Frommer, *Angew. Chem., Int. Ed. Engl.*, 1992, **31**, 1298.
46 D. M. Cyr, B. Venkataraman and G. W. Flynn, *Chem. Mater.*, 1996, **8**, 1600.
47 L. C. Giancarlo and G. W. Flynn, *Annu. Rev. Phys. Chem.*, 1998, **49**, 297.
48 A. Gesquière, M. M. S. Abdel-Mottaleb, S. De Feyter, F. C. De Schryver, F. Schoonbeek, J. van Esch, R. M. Kellogg, B. L. Feringa, A. Calderone, R. Lazzaroni and J. L. Brédas, *Langmuir*, 2000, **16**, 10 385.
49 S. De Feyter, A. Gesquière, P. C. M. Grim, F. C. De Schryver, S. Valiyaveettil, C. Meiners, M. Sieffert and K. Müllen, *Langmuir*, 1999, **15**, 2817.
50 S. De Feyter, P. C. M. Grim, M. Rücker, P. Vanoppen, C. Meiners, M. Sieffert, S. Valiyaveetiil, K. Müllen and F. C. De Schryver, *Angew. Chem., Int. Ed. Engl.*, 1998, **37**, 1223.
51 S. De Feyter, A. Gesquière, F. C. De Schryver, C. Meiners and K. Müllen, *Langmuir*, 2000, **16**, 9887.
52 A. Stabel, R. Heinz, F. C. De Schryver and J. P. Rabe, *J. Phys. Chem.*, 1995, **99**, 505.
53 A. Stabel, H. Heinz, J. P. Rabe, G. Wegner, F. C. De Schryver, D. Corens, W. Dehaen and C. Süling, *J. Phys. Chem.*, 1995, **99**, 8690.
54 A. Gesquière, M. Abdel-Mottaleb and F. C. De Schryver, *Langmuir*, 1999, **15**, 6821.
55 A. Gesquière, M. Abdel-Mottaleb, S. De Feyter, F. C. De Schryver, M. Sieffert, K. Müllen, A. Calderone, R. Lazzaroni and J. L. Brédas, *Chem. Eur. J.*, 2000, **6**, 3739.
56 S. De Feyter, K. Grim, J. van Esch, R. M. Kellogg, B. L. Feringa and F. C. De Schryver, *J. Phys. Chem. B*, 1998, **102**, 8981.
57 R. Heinz, A. Stabel, J. P. Rabe, G. Wegner, F. C. De Schryver, D. Corens, W. Dehaen and C. Süling, *Angew. Chem., Int. Ed. Engl.*, 1994, **33**, 2080.
58 P. Vanoppen, P. C. M. Grim, M. Rücker, S. De Feyter, G. Moessner, S. Valiyaveettil, K. Müllen and F. C. De Schryver, *J. Phys. Chem.*, 1996, **100**, 19636.
59 P. C. M. Grim, S. De Feyter, A. Gesquière, P. Vanoppen, M. Rücker, S. Valiyaveettil, G. Moessner, K. Müllen and F. C. De Schryver, *Angew. Chem., Int. Ed. Engl.*, 1997, **36**, 2601.
60 S. De Feyter, A. Gesquière, M. M. Abdel-Mottaleb, P. C. M. Grim, F. C. De Schryver, C. Meiners, M. Sieffert, S. Valiyaveettil and K. Müllen, *Acc. Chem. Res.*, 2000, **33**, 520.
61 V. Enkelmann, *Adv. Polym. Sci.*, 1984, **63**, 91.